Electronic structure of δ-doped quantum wells

Mao-long Ke and B. Hamilton
Department of Pure and Applied Physics, The University of Manchester Institute of Science and Technology, Manchester M60 1QD, United Kingdom
(Received 29 May 1992; revised manuscript received 5 October 1992)

We present self-consistent calculations of the electronic structure of δ-doped quantum wells. The sensitivity of the energy levels to various parameters—including impurity concentration, impurity spread, well width, and temperature—is examined. The effect of the finite barrier thickness is also considered, in order to ascertain the degree of carrier transfer into the surrounding material as a function of well width, barrier thickness, and impurity concentration.

I. INTRODUCTION

There is a growing interest in the use of the δ- (or atomic plane) doping technique to introduce carrier confinement effects. In the case of a single δ sheet in bulk GaAs, theoretical investigation of the electron energy levels has been made by several groups.[1–4] The existence of confined subbands and a two-dimensional (2D) electron gas has been predicted in the calculations, and the predictions have been confirmed by experimental techniques such as infrared absorption,[5] Raman scattering,[6,7] and magnetotransport measurements.[8–10]

For δ-doped quantum wells in the GaAs/$Al_xGa_{1-x}As$ system, several recent reports have described their experimental behavior. Both transport[11,12] and optical properties[13,14] of δ-doped quantum wells have been shown to depend on the dimensionality of the structures. However, the electronic structure for the δ-doped quantum wells has not, to our knowledge, been published in detail so far.

In this Brief Report, we present detailed calculation results for such a hybrid δ-heterojunction system by solving the Schrödinger and Poisson equations self-consistently for different temperatures. The effects of impurity diffusion in the growth direction are considered, and our calculations have been made for a range of impurity concentrations and quantum-well widths. We also calculate the influence of the barrier thickness, from which we have been able to determine the significance of electron transfer into buffer or capping layers.

Many-body effects, such as exchange and correlation, have been included in our calculations but produce only very small changes in the shape of the potential, in agreement with previous observations.[3] Many-body effects do, however, exert a characteristic rigid shrinkage of the gap in the type of the structure discussed here. Calculation of band-gap renormalization in similar structures will be presented separately.

II. PHYSICAL DESCRIPTION AND NUMERICAL RESULTS

A. Physical description

In the heavily doped regime, the average impurity separation is comparable to, or even less than, twice the effective Bohr radius (a_B^*), which enables coupling between impurity states. Consequently, electrons are unable to localize at a particular impurity atom even at zero temperature. The associated disappearance of the donor binding energy at high doping concentration is a common characteristic of III-V materials.[15,16] Theoretically, the systems of interest here can be analyzed as the response of a metalliclike 2D electron gas (2DEG) to the confining potential caused both by the heterointerfaces and the ionized impurity sheet. In other words, the degenerate 2D electrons will screen out, at least partially, the total confining potential and lead to a progressive reshaping of the well.

The theoretical model and equations used in this calculation are essentially the same as those for calculating the single δ sheet in the bulk GaAs,[1,3] except that there is an extra potential in the Schrödinger equation due to the presence of the heterointerfaces. The conduction- to valence-band offset ratio is assumed to be 65 to 35 (Ref. 17) in the calculation. The electron effective masses used are $0.067m_0$ for GaAs and $(0.067+0.083x)m_0$ for $Al_xGa_{1-x}As$ (Ref. 18) and the effective discontinuity at the interfaces has been accounted with appropriate boundary conditions.[19] A dielectric constant of 13.1 was chosen for both GaAs and $Al_xGa_{1-x}As$.

B. Numerical results

1. Structures with infinite barrier width

We first consider a system which has an *n*-type center δ-doped GaAs well grown between two infinitely wide $Al_{0.3}Ga_{0.7}As$ barriers. The background impurities in $Al_xGa_{1-x}As$ barriers are assumed to be acceptors at a level of 10^{15} cm^{-3}, and the δ-doped impurities are assumed to distribute homogeneously over an area with a thickness of δz.

We have solved the Schrödinger and Poisson equations self-consistently, and the results for zero temperature are presented first. For ideal δ sheets ($\delta z \rightarrow 0$), the calculated electron energy levels at different concentrations are shown in Fig. 1 for a well width of 120 Å. The hatched area is occupied by the two-dimensional electron gas.

The conduction-band potentials are presented in Fig. 2(a) for four different well widths w_d (50, 100, 200, and

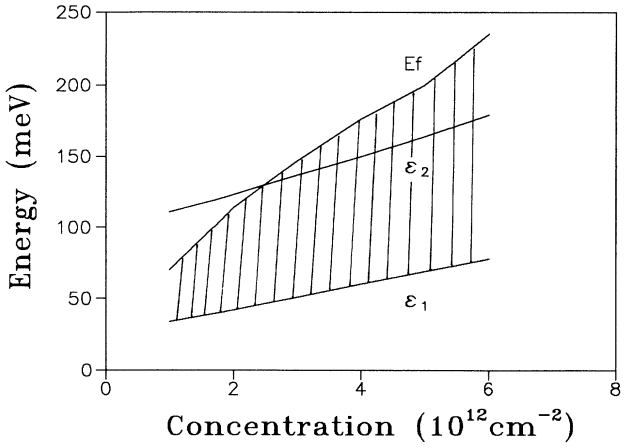

FIG. 1. Calculated electron energy levels and Fermi level as a function of δ sheet concentration, for a center doped $GaAs/Al_{0.3}Al_{0.3}Ga_{0.7}As$ quantum well with a well width of 120 Å. The hatched area is occupied by electrons.

400 Å), at a fixed δ concentration of 5×10^{12} cm^{-2}. The corresponding electron density profiles are shown in Fig. 2(b). For very large compositional well widths, the systems are essentially δ-doped double heterostructures; the compositional band offsets do not influence the single δ potential. As the well width reduces, the two potentials interact and the electrons redistribute. The final potential becomes an interacted cusplike quantum well. It is interesting to note that the electron density profile (measured by the full width at half maximum) is less sharp for a well width of 200 Å than for a well width of 400 Å. This is because the ground state, which has a higher electron population in the wider well widths, is also better confined to the δ-doping potential. The uppermost excited state population in the wider well contributes to an electron density tail spread across the whole well.

The effect of impurity spread has been illustrated in Fig. 3 for the same sheet donor concentration (5×10^{12} cm^{-2}) and a well width of 200 Å. Figure 3(a) shows the effective potentials for four different uniform impurity spreads with δz equal to 2, 50, 100, and 150 Å. The corresponding electron density profiles are shown in Fig. 3(b). The interesting double-peaked electron distributions which evolve as δz increases can be understood in the following way. As δz increases, the potential in the bottom of the well becomes flat; this reduces the intersubband spacing and increases the electron population in the $n=2$ subband, which contributes zero electron density at the center of these symmetrical structures.

When the temperature is raised from 0 to 300 K, the subband populations will change according to the Fermi-Dirac statistics. Furthermore, the total band bending z_A will also be affected because of the different Fermi-level position relative to the bottom of the conduction band in the region remote from the degenerate electron gas. Generally speaking, the electron energy levels increase slowly and smoothly as the subband occupancy changes modify the impurity screening. The electron population de-

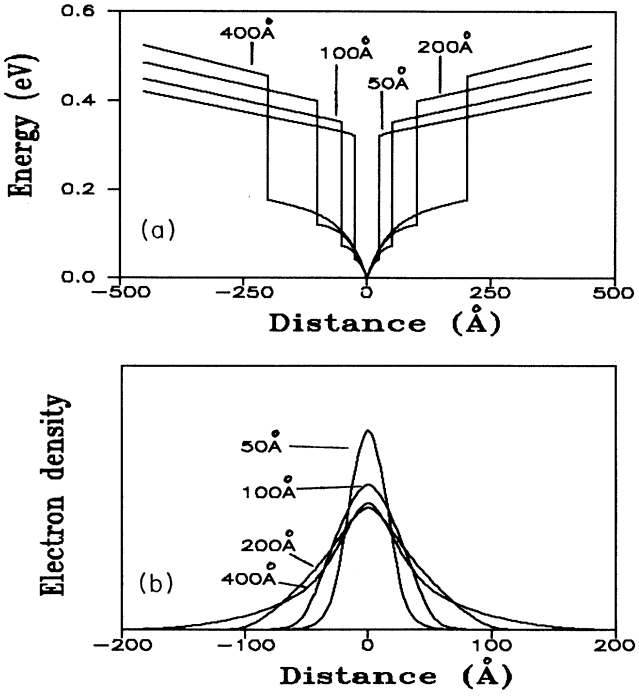

FIG. 2. (a) displays the conduction-band potentials for four different well widths (w_d): 50, 100, 200, and 400 Å, at a fixed δ sheet concentration of 5×10^{12} cm^{-2}. The corresponding electron density profiles are shown in (b).

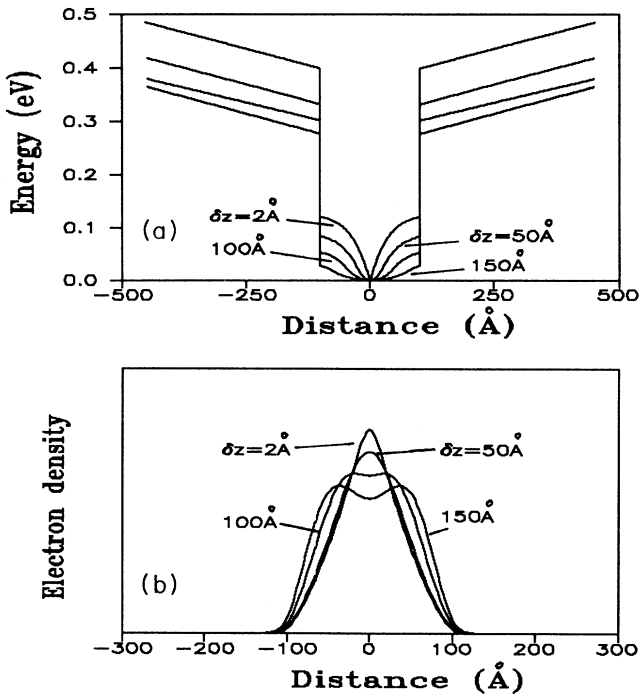

FIG. 3. (a) shows the conduction-band potentials for four different uniform impurity spreads with δz equal to 2, 50, 100, and 150 Å at a fixed δ sheet concentration of 5×10^{12} cm^{-2}. The corresponding electron density profiles are presented in (b).

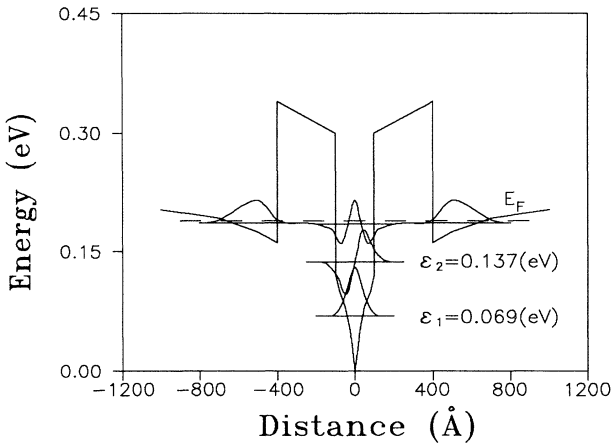

FIG. 4. Calculated potential, wave functions, and the energy levels for barrier widths of 300 Å and a well width of 200 Å at a fixed δ concentration of 5×10^{12} cm^{-2}.

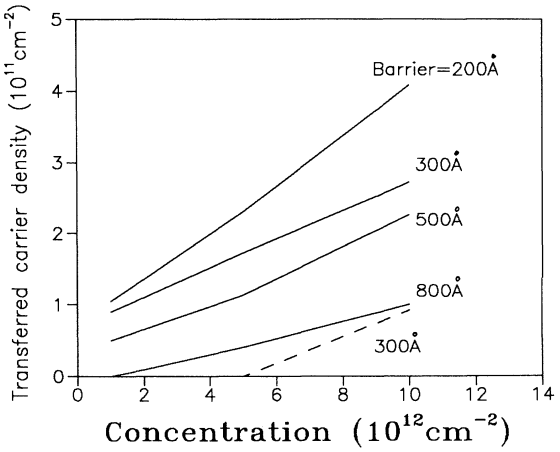

FIG. 5. Variation of carrier concentration in the buffer and capping layers as a function of impurity concentration, barrier width, and well width. The solid lines are the result for a fixed well width of 200 Å, but with different barrier thicknesses (shown in the figure). The broken line is the result for a well width of 500 Å and a barrier thickness of 300 Å.

creases noticeably for the ground state ($n=1$) and less dramatically for the $n=2$ state. The occupancy of the highest state ($n=3$) increases during the temperature change.

2. *Structures with finite barrier width*

In practical sample preparation, a buffer layer is normally grown before the quantum well in order to improve its quality, and a capping layer is deposited after the quantum-well growth for protection. The finite barrier width in any real crystal has an important effect on the degenerate carriers inside the well due to the requirement of an equal Fermi level through the entire system in equilibrium condition. A small fraction of the 2D electron gas will distribute beyond the barriers in order to raise the Fermi level in the buffer or capping regions. This carrier transfer has two important consequences: first, it reduces the 2D electron density and lowers the Fermi level inside the well region; second, it decreases the total electron screening potential due to the increase of the average distance between the electron gas and the impurities. Figure 4 illustrates the calculated potential, wave function, and energy levels for barrier widths of 300 Å and a well width of 200 Å (the aluminum fraction x remains at 0.3).

Figure 5 quantifies the degree of carrier transfer into the buffer and capping sides as a function of impurity concentration, barrier width, and well width. In keeping with intuition, high impurity concentrations lead to greater carrier transfer provided that other parameters remain unchanged. Narrow barriers result in greater electron transfer because they limit the degree of band bending (for a given electron transfer) available for Fermi-level alignment. Narrower wells also promote electron transfer mainly due to the associated raising of the Fermi level inside the well; the result for a very wide well (500 Å) with 300-Å barriers, shown in Fig. 5, illustrates this effect.

III. CONCLUSIONS

We have investigated the electronic structure of center δ-doped quantum wells both with infinite and finite barrier thickness (or width). In the case of infinite barrier width, the change of electron energy levels as a function of impurity concentration, impurity spread, well width, and temperature has been examined. The shape of the potential and the energy levels are generally very sensitive to all the parameters involved in the calculation. Several unusual features emerge for these systems. The electron distribution in the confinement direction shows a double-peak structure when the δ-doping sheet spread approaches 100 Å. The half-width of the distribution, however, is smaller for a 400-Å-wide well than for a 200-Å-width structure. The effect of the finite barrier thickness has also been studied. The requirement of equal Fermi level for the whole structure at thermal equilibrium forces a certain amount of carrier transfer from the well forming a 2DEG sheet in the buffer and capping regions adjacent to the barriers. We have quantified the degree of the electron transfer as a function of barrier width, well width, and impurity concentration.

ACKNOWLEDGMENTS

The authors gratefully acknowledge the support of the SERC for this work. We would also like to thank M. Godfrey, P. Dawson, and J. Rimmer for helpful discussions and comments.

[1]A. Zrenner, F. Koch, and K. Ploog, Surf. Sci. **196**, 671 (1988).
[2]E. F. Schubert, T. H. Chiu, J. E. Cunningham, B. Telland, and J. B. Stark, J. Electron. Mater. **17**, 527 (1988).
[3]M. H. Degani, Phys. Rev. B **44**, 5580 (1991).
[4]L. Ioriatti, Phys. Rev. B **41**, 8340 (1990).
[5]N. Schwarz, F. Muller, G. Tempel, F. Koch, and G. Weiman, Semicond. Sci. Technol. **4**, 571 (1989).
[6]G. Abstreiter, R. Merlin, and A. Pinczuk, IEEE J. Quantum Electron. **QE-22**, 1771 (1986).
[7]J. Wagner, A. Fisher, and K. Ploog, Phys. Rev. B **42**, 7280 (1990).
[8]F. Koch and A. Zrenner, Mater. Sci. Eng. B **1**, 221 (1989).
[9]A. Zrenner, F. Koch, R. L. Williams, R. A. Stradling, K. Ploog, and G. Weimann, Semicond. Sci. Technol. **3**, 1203 (1988).
[10]M. Santos, T. Sajota, A. Zrenner, and M. Shayegan, Appl. Phys. Lett. **53**, 2504 (1988).
[11]W. Ted Masselink, Phys. Rev. Lett. **66**, 1573 (1991).
[12]W. Ted Masselink, Appl. Phys. Lett. **59**, 694 (1991).
[13]Mao-long Ke, J. S. Rimmer, B. Hamilton, J. H. Evans, M. Missious, K. E. Singer, and P. Zalm, Phys. Rev. B **45**, 14 114 (1992).
[14]C. I. Harris, H. Kalt, and B. Monemar (unpublished).
[15]N. F. Mott and W. D. Twose, Adv. Phys. **10**, 107 (1961).
[16]H. C. Casey, Jr. and M. B. Panish, *Heterostructure Lasers* (Academic, London, 1978), Pt. A, pp. 131–133.
[17]P. Dawson, K. J. Moore, G. Duggan, H. I. Ralph, and C. T. B. Fox, Phys. Rev. B **34**, 6007 (1986).
[18]H. C. Casey, Jr. and M. B. Panish, *Heterostructure Lasers* (Ref. 16), p. 192.
[19]R. Lassnig, Phys. Rev. B **31**, 8076 (1985).